

Revisiting the 1897 Shillong and 1905 Kangra earthquakes in northern India: Site response, Moho reflections and a triggered earthquake

Susan E. Hough^{1,*}, Roger Bilham², Nicolas Ambraseys³ and Nicole Feldl²

¹United States Geological Survey, 525 S. Wilson Avenue, Pasadena, CA 91106, USA

²Department of Geological Sciences, University of Colorado, Boulder, CO 80309, USA

³Department of Earthquake Engineering, Imperial College, London SW7 2AZ, UK

Re-evaluated intensity distributions for the 1897 M_w 8.0 Shillong and the 1905 M_w 7.8 Kangra earthquakes, combined with geodetic constraints on rupture geometries, allow us to compare observed distributions of intensity with theoretically predicted shaking. The difference between predicted and observed shaking is interpreted in terms of the site response of the Ganges and Brahmaputra basins. These comparisons identify regions of enhanced shaking along main rivers, revealing amplifications of 1–2 intensity units, roughly an amplification of 2–4 in acceleration. We also find two unexpected results in our analysis of the Kangra earthquake: (i) The epicentral region is surrounded by a halo of enhanced intensity at 150–200 km radius and (ii) The Dehra Dun region was the locus of a broad region of anomalously high intensities. We interpret the former result as the signal from post-critical Moho reflections and the latter observation as a probable second large earthquake ($M > 7$) at 30–50 km depth triggered within minutes of the 1905 main shock. These results have important consequences from future earthquakes in the Himalaya.

SEVERAL recent studies have provided new estimates of magnitude, rupture parameters, and shaking intensity for the 1897 Assam and the 1905 Kangra earthquakes in northern India. The dense spatial coverage of these data provides substantial information about the distribution of shaking in the alluvial plains of northern India that can be used to evaluate past and future great Himalayan earthquakes as well as to address unresolved general issues related to both events.

The magnitudes of the 1897 and 1905 earthquakes listed in early catalogues vary by 0.5 magnitude units. The re-evaluated instrumental data indicate the 1897 earthquake¹ was $M_s = 8.0 \pm 0.1$, and the 1905 earthquake² was $M_s = 7.8 \pm 0.05$.

The observed shaking intensity distribution for the 1897 earthquake was originally evaluated by Oldham³, and for the 1905 earthquake by Middlemiss^{4,5}. These observations have now been supplemented by additional accounts found in newspapers, government reports and other materials, and these have been re-evaluated using the MSK scale. In all

282 unequivocal MSK intensities were assigned for the 1897 earthquake (Figure 1 *a*)⁶, and 523 for the 1905 earthquake (Figure 1 *b*)⁷. The new evaluations take into account building styles and ignore accounts for which reliable intensities cannot be assessed. In particular, locations where damage was associated with liquefaction were not included in assessments of intensity. Liquefaction tends to occur on saturated sediments over a range of moderate to high intensities, resulting in building damage caused by foundation failure, rather than by direct shaking effects. It is typically impossible to assign a precise intensity to these observations.

Rupture geometry for the 1897 and 1905 earthquakes

Geodetic and geological data provide strong constraints on rupture geometry of the 1897 Shillong earthquake, indicating 16 ± 5 m of reverse slip on a 110 ± 10 km ESE fault⁸, corresponding to $M_w = 8.1 \pm 0.1$. The rupture appears to have slipped on a $50 \pm 5^\circ$ SSW dipping fault from 35 to 9 km depth, extending through much of the crust. This subsurface slip stressed the shallower regions of the Shillong plateau resulting in 10 m of normal faulting on the Che-drang fault³.

In contrast, geodetic data for the Kangra earthquake sample only the SW edge of the inferred 1905 rupture and provide weak constraints for an inferred shallow-dipping thrust fault with less than 5 m of slip⁹. Several authors have used leveling data from the Dehradun region to support the notion that rupture extended 250 km SE of the epicenter, consistent with a region of high intensity shaking recorded in the region of Dehradun (e.g. most recently ref. 10). A re-evaluation of the raw leveling data shows, however, that the leveling data are significantly contaminated by errors¹¹ and that there was probably little or no uplift in the Dehradun region. The absence of significant deformation at Dehradun constrains the rupture length to be less than 180 km. This is consistent with the revised magnitude of $M_w = 7.8$, which suggests the rupture length was no more than 110 km (ref. 9). The rupture presumably terminated to the southwest near the mapped location of the Jawalmucki thrust fault¹². The inferred rupture parameters for 1897 and

*For correspondence. (e-mail: hough@usgs.gov)

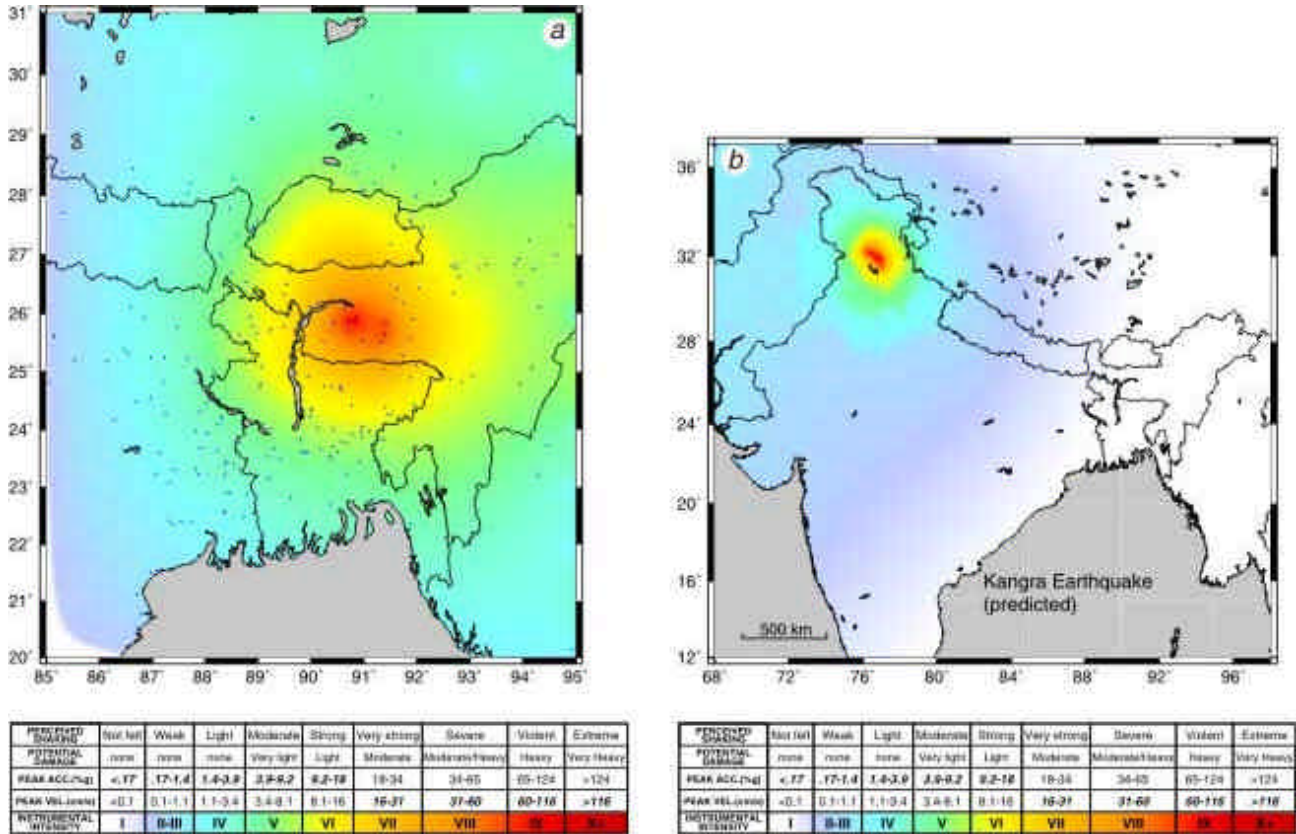


Figure 1. Observed intensity distribution for the (a) 1897 Assam earthquake and (b) 1905 Kangra earthquake as determined by Ambraseys and Bilham⁶ and Ambraseys and Douglass⁷, respectively. Scale bar indicates ground motion values, pga and pgv, that are found to correspond to each intensity level using instrumentally recorded earthquakes in California.

1905 are used below as input in computer simulations that generate synthetic shaking intensity maps for each earthquake.

Previous attempts to assess the location, extent and strike of the 1905 rupture area based on published intensity⁵ show a zone of intense destruction near the town of Kangra (RF VIII-X), and an isolated zone of lower intensity (RF VIII) ~250 km to the SW near Dehradun. For many years the early magnitude estimates supported the widely held belief that the rupture zone corresponded approximately to the area of RF intensity VII shaking that enveloped these two regions.

The reality of the intervening region of lower intensity shaking between these two regions of damage was investigated by previous studies^{13,14}. These studies conclude that Middlemiss's coverage of the intervening region would have revealed high intensity shaking had any been present. The revised and expanded MSK data confirm that the low intensity region is not an artifact of poor spatial sampling (Figure 1 b).

We contoured the reevaluated MSK distribution using a mathematical algorithm. Contouring is done using the GMT routine 'surface'¹⁵; this routine produces contours of randomly spaced spatial data, $z(x, y)$, by solving

$$(1 - T) \cdot L(L(z)) + T \cdot L(z) = 0,$$

where T is a tension factor and L is the Laplacian operator. We use $T = 1$, which provides a harmonic solution with no maxima or minima away from control points. Our contours resemble the older Rossi-Forel isoseismals, although our larger number of intensity reports reveals additional detail. The contours in Figure 1 b confirm the low intensity region separating the epicentral rupture zone from a zone of high intensity near Dehra Dun.

Middlemiss' higher isoseismals tend to include unjustifiably large areas, a conclusion derived also for Oldham's isoseismals contoured for the 1897 earthquake⁶. This bias is caused by extensive building damage at relatively modest levels of shaking. A comparison of Middlemiss' areas of Rossi-Forel shaking with those of inferred MSK shaking shows them to be approximately one intensity unit too high above Intensity VIII and a half intensity too high above intensity VII. For lower intensities we find the areas comparable.

Predicted intensity distributions

One can use modern modelling methods to predict the distribution of ground motions from a given fault model and, using established relationships between ground motions and

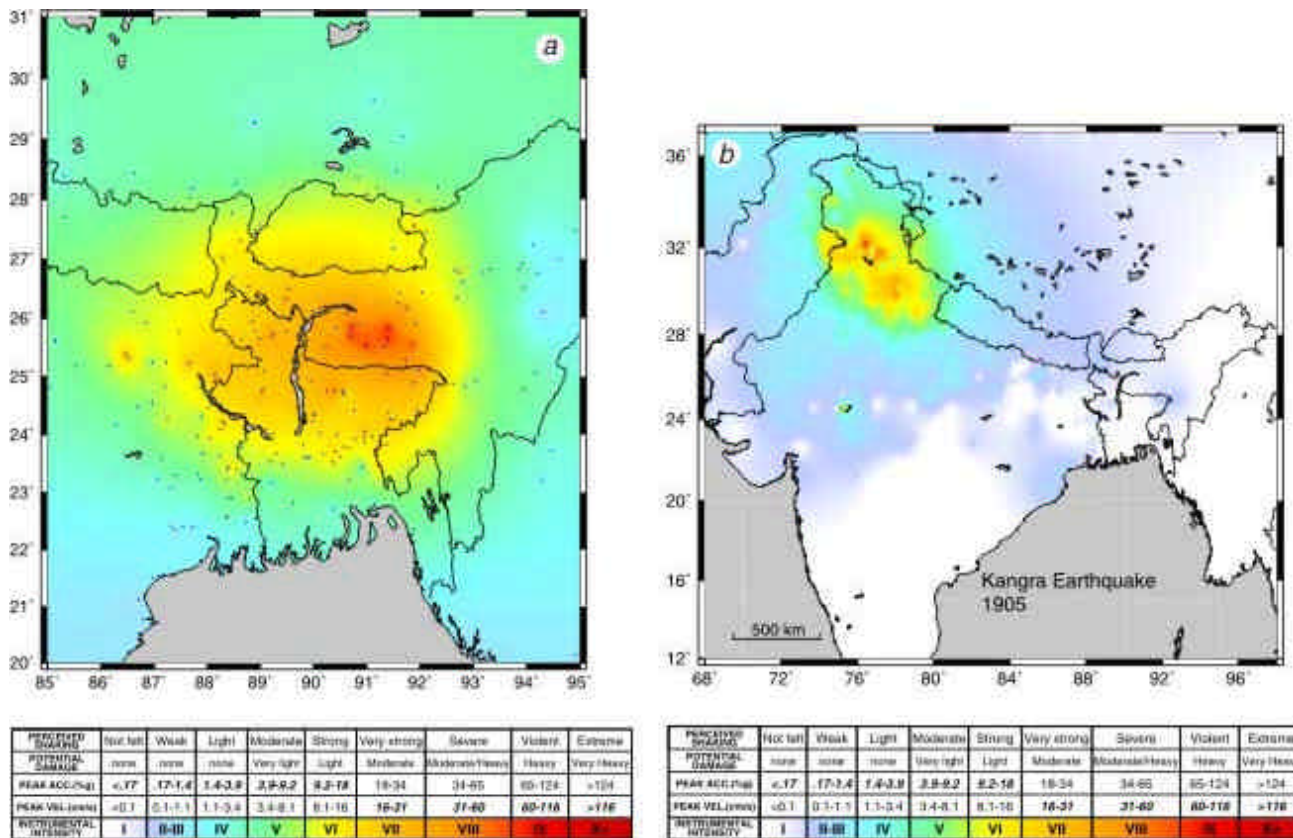


Figure 2. Predicted shaking intensity from the (a) 1897 Assam earthquake and (b) the 1905 Kangra earthquake determined using methodology and rupture models discussed in the text. These maps are drawn from predicted pga values, which are converted to intensity using the values given in the scale bar.

intensities¹⁶, convert this into a predicted damage map¹⁷. We calculate predicted hard-rock damage patterns from both the 1897 and the 1905 earthquakes using rupture models constrained from geodetic data and other available information. We use a well-calibrated, semi-stochastic approach that includes finite-fault effects to the extent that the source is distributed, although finite-fault phase effects are not modeled with this approach¹⁸. We also use the attenuation results of Singh *et al.*¹⁹ for regional $Q(f)$.

One key unknown in the modelling approach is the ‘strength factor,’ which is related to slip velocity¹⁸. For both earthquakes we initially choose the same value obtained previously for the Bhuj earthquake: 1.6 (ref. 17). Although this value cannot be determined precisely without quantified ground motion estimates, it can be adjusted based on the overall intensity pattern. For the 1897 earthquake, we find that the value of 1.6 provides a very good fit to the extent of the region over which light damage occurred. For the 1905 earthquake, a better fit is obtained with a lower value: 1.2. To include the effect of the Chedrang fault rupture in our predicted shaking map for the Assam earthquake, we model a second event with the appropriate rupture parameters. The combined intensity map is then determined by choosing, at each point, the higher of the values predicted from the Chedrang and Oldham fault ruptures. This approach presumably provides a lower bound for the combined shaking

level, as two distinct ruptures are expected to prolong the duration of strong ground motion at many sites, and thus to potentially generate more severe damage than two distinct earthquakes.

Figure 2a, b shows the observed and predicted intensity distributions for the 1897 and 1905 earthquake. Figure 3a, b shows the residuals: calculated simply as the observed minus predicted intensity values.

For the Shillong earthquake, we obtain a broad region of amplified intensities corresponding to the Ganges Basin (Figure 3a), consistent with the expectation of amplification at soft-sediment sites. We do not observe amplification along the Brahmaputra River, but this is because intensity values are not assigned for the many sites along this river for which there was documented liquefaction, but insufficient information to assign intensity⁶. Many of the liquefaction sites are along the Brahmaputra River (Figure 3a); it thus appears that shaking was amplified in these locations as well, although the observations are not sufficient to quantify it. Throughout the Ganges Basin, however, we find consistent amplification of 1–2 intensity units, implying a peak ground acceleration amplification of 2–4 (ref. 17).

The intensity residuals from the 1905 earthquake reveal a more complex pattern than those from the 1897 event (Figure 3b). Our preferred choice of strength factor results in a good overall match to the shaking distribution. However,

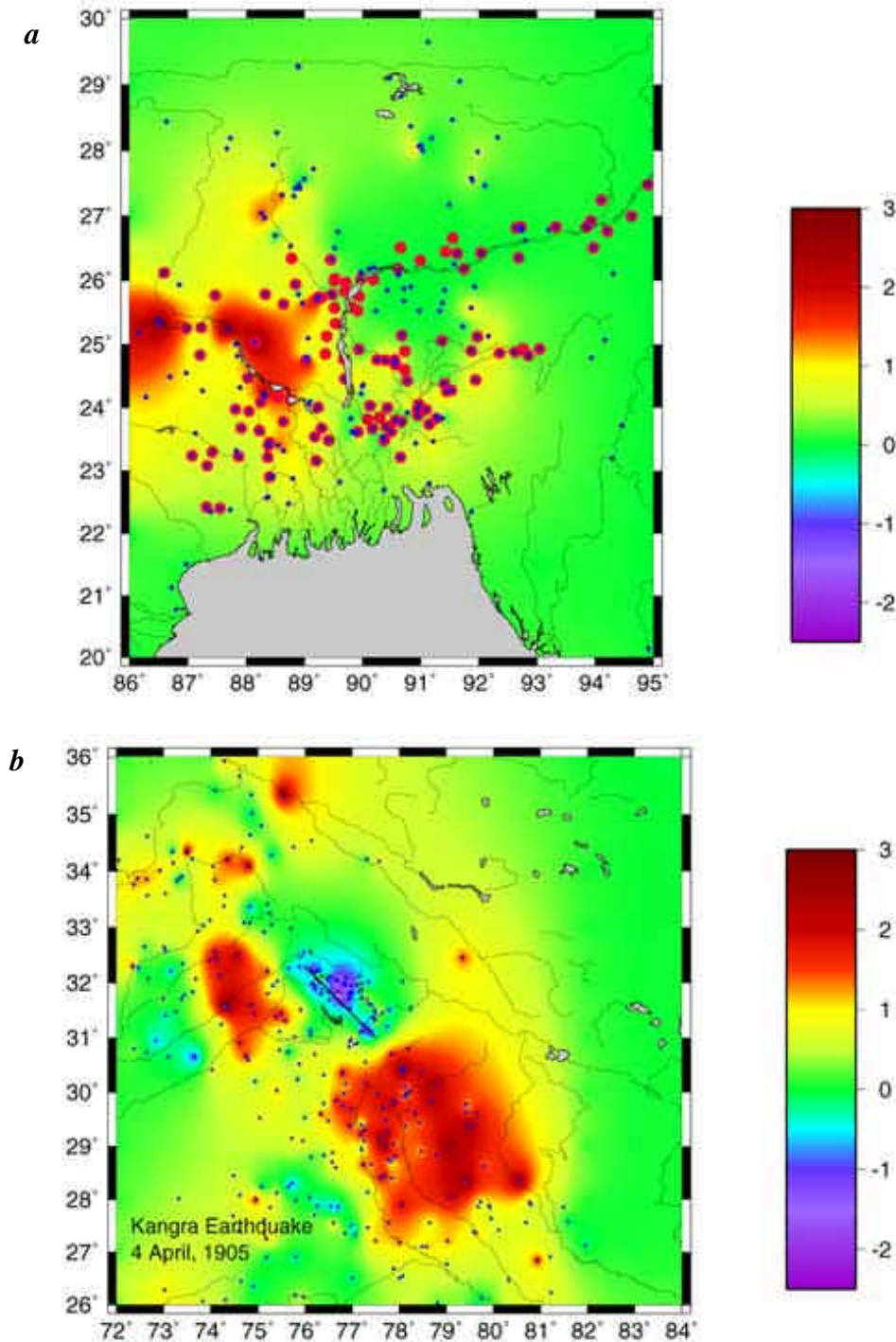


Figure 3. Residual intensity (observed minus predicted) from the (a) 1897 Assam earthquake and (b) the 1905 Kangra earthquake determined using methodology and rupture models discussed in text. Red circles indicate sites at which liquefaction was documented. Small circles in both panels indicate locations at which intensity values were determined. The same scale bar (far left) is used to generate both figures.

several features of the residual map are found to be insensitive to changes in modelling parameters.

We make the following observations: (i) Shaking in the main rupture zone is over predicted, (ii) amplified shaking is observed near the banks of rivers in the Ganges, and in the Kashmir Valley, (iii) a faint region of increased intensity is evident surrounding the epicenter at a distance of roughly

180 km, and (iv) a broad region of high residuals is found near Dehradun; this is displaced 20 km to the east from a high intensity zone contoured by Middlemiss. These observations are discussed below.

Our modelling predicts stronger near-field shaking than that observed in the Kangra region. It is possible that this reflects a bias in the intensity assignments: if the only

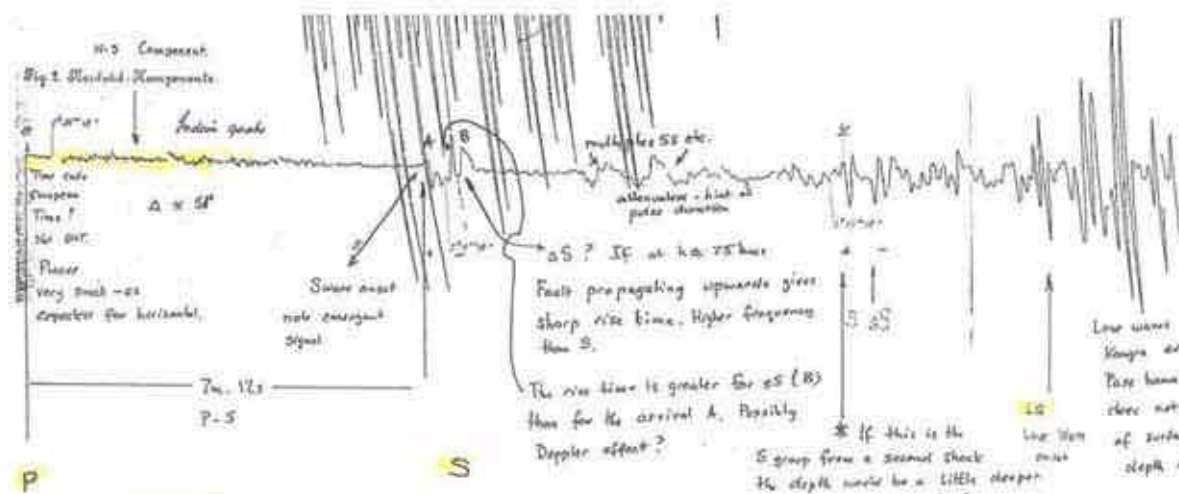


Figure 4. Recording of the 1905 Kangra mainshock made by an early Wiechert seismometer in Leipzig, Germany. The record reveals a clear initial S/S arrival, followed by S-wave multiples with longer periods. About 7 minutes after the first S/S arrivals, a second apparent S/S group arrives ahead of the surface waves. The high frequency character of the second S-wave group is consistent with primary body wave arrivals from a second event but not with S-wave multiples from the first event. The second S/S group reveals a greater S-s time than the initial S-wave group, suggesting the second event was deeper than the first.

structures damaged in an earthquake are of construction types that are highly vulnerable to damage, it is impossible to ascertain if very high shaking occurred. However, the 1905 main shock is inferred to have been a low-angle thrust rupture of the main Himalayan decollement fault, and several recent studies suggest that other shallow thrust events, most notably the 1999 Chi-Chi, Taiwan earthquake, generated relatively low near-field peak accelerations (e.g. ref. 20). Our results are consistent with this hypothesis.

Our second observation, of amplified shaking along rivers and in valleys, is again consistent with expectations for significant amplifications at soft-sediment sites. The degree of amplification is consistent with that inferred for the 1897 earthquake.

The faint high-intensity ‘halo’ surrounding the main shock extends both to the west of the main shock, on sediment sites, and to the east, on hard-rock sites. We interpret this pattern as evidence that post-critical Moho reflections are large enough to contribute in a significant way to damage patterns (Figure 4). Previous studies have argued for such an effect in other earthquakes beginning with the 1989 Loma Prieta, California earthquake²¹. Somerville and Yoshimura showed that SmS arrivals were larger than the direct S arrivals at distances of 50–100 km; later studies (e.g. ref. 22) have found similar results. Although a detailed crustal model would be required for precise ray-tracing, tomographic studies indicate that the Moho is located at approximately 40 km along the Himalayan front²³; high amplitude SmS waves at distances of 100–200 km are thus consistent with this interpretation.

While a number of studies have found evidence that post-critical Moho reflections contribute to damage patterns, past studies have relied on far fewer data points than are provided by our dense sampling. Perhaps, for the

first time, dense macroseismic data have illuminated the full spatial distribution of SmS arrivals. These results suggest a deeper Moho to the northeast of the main shock than to the southwest, a hypothesis that will be testable when crustal structure is known in more detail.

A faint halo is suggested in the intensity residuals calculated for the 1897 earthquake, especially to the south and west of the epicenter. The signal is less prominent, however, than that of the 1905 earthquake, presumably due to the latter event’s substantially deeper epicenter and different mechanism.

Perhaps the most conspicuous feature in the residual 1905 intensity plot is the roughly circular region of high intensities near Dehradun, centered slightly to the west of Middelmess’ intensity VIII outlier. The circular nature of the intensity pattern is suggestive of a triggered earthquake rather than sedimentary basin amplification since at least half of the high intensity observations are found north of the Ganga Plain within the Himalayan foothills. A second earthquake in the Dehradun region has been suggested by previous authors based on the Rossi–Forel intensity contours (e.g. ref. 24). Had a separate shock occurred it would have to have been close to the time of the main shock for people to not have reported two separate shocks. The epicenter of this triggered earthquake is apparently 29.0°N, 78.7°E with an uncertainty of ± 0.5°.

Although the intensity residual generated by the (inferred) triggered earthquake is dramatic, the intensity distribution reveals a broad region of relatively modest shaking in the Dehradun region. Using our modelling approach to match this pattern, we conclude that the earthquake must be large (M_w upwards of 7.0) and deep (depth upwards of 30 km). There is, however, a trade-off in the modelling between magnitude and depth; we cannot distinguish between, say,

a M_w 7 event at 30 km depth and a M_w 7.5 event at 50 km depth.

If a remotely triggered earthquake of $M_w \sim 7$ did occur at 30 km depth, the relatively recent 1988 Bihar–Nepal earthquake might represent an analog for this event. The PDE magnitude of this earthquake is M_w 6.7 and it occurred on a NE-trending strike-slip fault near the base of the India plate^{25–27}. The poor-quality geodetic data do not allow us to test the possible occurrence of a triggered earthquake near Dehradun. The leveling data are especially unhelpful to resolve the parameters of a deep earthquake, for which the surface deformation will be muted, and will be expressed by a long surface wavelength.

We searched for early instrumental recordings of the 1905 earthquake. Although instrumental recordings from this date are sparse, we were able to locate several records from which arrivals can be identified with some confidence. Two P -wave arrivals are evident at Colaba Observatory (Bombay) in the first minute of the earthquake, and two distinct S -wave arrivals separated by about 6–7 min are suggested in the Wiechert recording from Gottingham. The best evidence, however, comes from the station at Leipzig: a damped Wiechert instrument (Figure 5)²⁸. This record reveals clear evidence of a second, high-frequency S -wave group, about 7 min after the first S arrivals. The record moreover suggests that the sS - S time of the second event is larger than the sS - S time of the first event, consistent with our inference that the triggered earthquake was considerably deeper than the first. We note that a distinct sS - S group virtually requires the existence of a second, substantial earthquake.

An additional source of epicentral shaking data is found in the horizontal-force magnetogram recorded at Dehradun recorded on a chart advancing at approximately 15 mm/hour²⁹. The record saturates for 8 min following the arrival of surface waves from the main shock, but distinct shocks occur at 11.3, 19.7, 25.6 and 43.5 min after this first arrival. The reported times indicate the arrival of Raleigh waves at Dehradun at 00:51 \pm 1 m GMT²⁹. Middlemiss infers an origin time of 06:09 or 00:48.

Because of the initial saturation of the instrument, the data do not provide any information about separate shocks

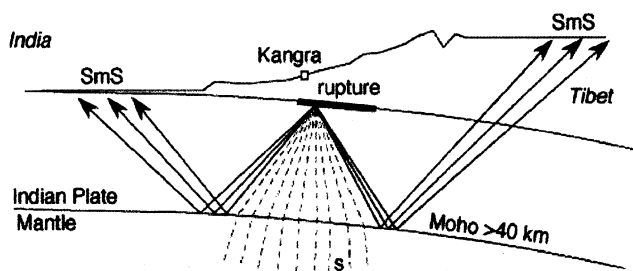


Figure 5. Cartoon illustrating the generation of post-critical SmS arrivals. If, as expected, the Moho thickens to the east of the mainshock, SmS arrivals are expected to be generated at greater distances in the Himalaya than in the direction of India.

that might have occurred within 8 min of the mainshock. However, the noted times of the later events can be used to constrain the times of early large aftershocks, which we use in the following section as a guide to the interpretation of anecdotal accounts.

Felt and recorded aftershocks in 1905

Numerous felt reports of aftershocks are listed by Middlemiss⁵ who considers their reported times to be unreliable. However, if we assume that observers noted only the strongest aftershocks, it is possible to synchronize these reports using the aftershocks recorded by the magnetogram. In Figure 6 we show the locations of reported aftershocks reported during the 15 min following the main shock. The mean location of reports (independent of intensity) for two consecutive 8 min windows are calculated to lie 20–100 km SE of Dehradun, near the inferred location of the second shock.

Because the Kangra epicentral region was severely damaged, few people were able to document the timing of aftershocks. The locations may thus be biased away from the

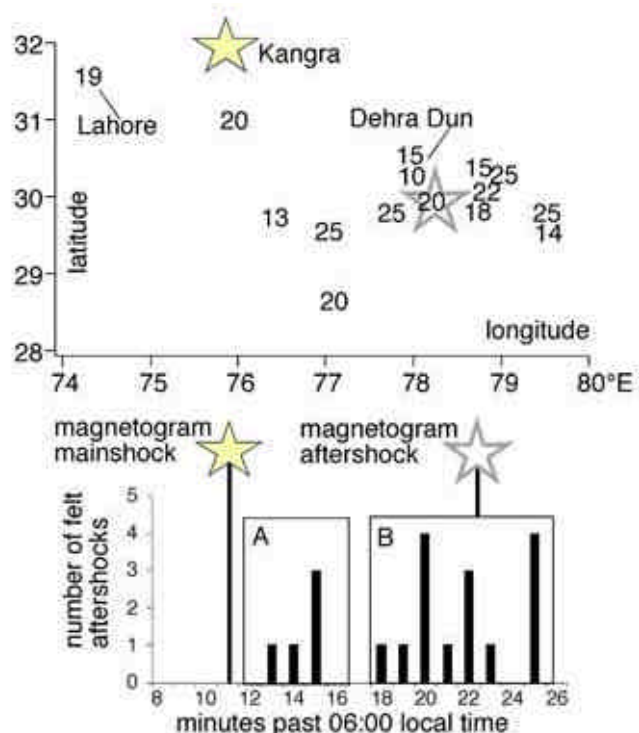


Figure 6. Map showing location and felt time in minutes of Kangra 'aftershocks'. Histogram below shows the clustering of these in time relative to the mainshock and aftershock recorded by a continuously recording magnetometer at Dehradun. The magnetogram saturated in the first 8 min, but a distinct arrival occurred 11.3 min after the mainshock. The mean and median locations for aftershocks reported in intervals A and B are all located within the star shown in map view ($77.3 \pm 0.5^\circ\text{E}$, $30 \pm 0.1^\circ\text{N}$). The 14 reports that may refer to the 11.3 min aftershock point to an epicenter at 78°E , 30°N , approximately 40 km SE of Dehradun.

main shock epicenter. Together with the scant distribution of quantitative observations and their concentration in a few urban centers, this leads to a probable bias toward Dehradun. Still, the results suggest that the Dehradun region experienced either an anomalously large number of felt aftershocks shortly after the main shock, or a large number of poorly timed observations of a single large aftershock, within fifteen minutes of the main shock arrival.

Conclusions

Macroseismic observations from two key historic earthquakes in the Himalayan region reveal unexpected details of the nature of the ground motions generated by these events. Using available rupture models, we are able to predict the distributions of shaking from the events and to compare these results to the observed intensities. We obtain several interesting results, including maps of sediment-induced amplification in the Ganges Basin and elsewhere, as well as compelling evidence that the 1905 Kangra main shock was followed by a subsequent, remotely triggered earthquake in the Dehradun region. The depth of this triggered earthquake (30–50 km) requires it to have occurred below the plate boundary, and probably at the base of the Indian plate. This result underscores two important conclusions about triggered earthquakes. First, while small remotely triggered earthquakes occur commonly in geothermal and volcanic regions (e.g. ref. 30), large triggered earthquakes are possible. This triggered earthquake, like the 1988 Udaypur, Nepal, earthquake, underscores the important conclusion that an important source of seismic hazards in the Himalaya lies not only on slip on the plate boundary, but from earthquakes at depth (e.g. ref. 31).

1. Ambraseys, N., Reappraisal of north-India earthquakes at the turn of the 20th century. *Curr. Sci.*, 2000, **79**, 1237–1250.
2. Ambraseys, N. and Bilham, R., A note on the Kangra $M_s = 7.8$ earthquake of 4 April 1905. *Curr. Sci.*, 2000, **79**, 101–106.
3. Oldham, Report of the great earthquake of 12 June 1897. *Mem. Geol. Surv. India*, 1899, p. 379.
4. Middlemiss, C. S., Preliminary account of the Kangra earthquake of 4 April 1905. *Mem. Geol. Soc. India*, 1905, **32**, 258–294.
5. Middlemiss, C. S., The Kangra earthquake of 4 April 1905. *Mem. Geol. Surv. India*, 1910, **38**, 405.
6. Ambraseys, N. and Bilham, R., Reevaluated intensities for the great Assam earthquake of 12 June 1897, Shillong, India. *Bull. Seismol. Soc. Am.*, 2003, **93**, 655–673.
7. Ambraseys, N. N. and Douglas, J., Magnitude calibration of north Indian earthquakes. *Geophys. J. Int.*, (in press).
8. Bilham, R. and England, P., Plateau pop-up during the great 1897 Assam earthquake. *Nature*, 2001, **410**, 806–809.
9. Wallace, K., Bendick, R., Bilham, R., Blume, F., Gahalaut, V. and Gaur, V., Geodetic constraint of the Kangra 1905 $M_s = 7.8$ rupture. *EOS, Trans. Am. Geophys. Union*, 2002, **83**, Abstract S12C-07.
10. Yeats, R. S., Nakata, T., Faraj, A., Fort, M., Mirza, M. A., Pandey, M. R. and Stein, R. S., The Himalayan frontal fault system. *Ann. Tect.*, 1992, **6**, 85–98.
11. Bilham, R., Slow tilt reversal of the Lesser Himalaya between 1862 and 1992 at 78°E, and bounds to the southeast rupture of the 1905 Kangra earthquake. *Geophys. J. Int.*, 2001, **144**, 1–23.
12. Powers, P. M., Lillie, R. J. and Yeats, R. S., Structure and shortening of the Kangra and Dehra Dun reentrants, Sub-Himalaya, India. *Geol. Soc. Am. Bull.*, 1998, **110**, 1010–1027.
13. Seeber, L. and Armbruster, J. G., Great detachment earthquakes along the Himalayan Arc and long-term forecasting. *Am. Geophys. Union*, 1981, **4**, 259–277.
14. Molnar, P., The distribution of intensity associated with the 1905 Kangra earthquake and bounds on the extent of rupture. *J. Geol. Soc. India*, 1987, **29**, 221.
15. Wessel, P. and Smith, W. H. F., Free software helps map and display data. *EOS, Trans. Am. Geophys. Union*, 1991, **72**, 441–445.
16. Wald, D. J., Quitoriano, V., Heaton, T. H. and Kanamori, H., Relationships between peak ground acceleration, peak ground velocity, and modified Mercalli intensity in California. *Earthquake Spectra*, 1999, **15**, 557–564.
17. Hough, S. E., Martin, S., Bilham, R. and Atkinson, G., The 26 January 2001 Bhuj, India earthquake: Observed and predicted ground motions. *Bull. Seismol. Soc. Am.*, 2002, **92**, 2061–2079.
18. Beresnev, I. A. and Atkinson, G. M., Generic finite-fault model for ground-motion prediction in eastern North America. *Bull. Seismol. Soc. Am.*, 1997, **89**, 608–625.
19. Singh, S. K., Ordaz, M., Dattatrayam, R. S. and Gupta, H. K., A spectral analysis of the 21 May 1997, Jabalpur, India earthquake (M_w 5.8) and estimation of ground motion from future earthquakes in the Indian shield region. *Bull. Seismol. Soc. Am.*, 1999, **89**, 1620–1630.
20. Boore, D. M., Comparisons of ground motions from the 1999 Chi-Chi earthquake with empirical predictions largely based on data from California. *Bull. Seismol. Soc. Am.*, 2001, **91**, 1212–1217.
21. Somerville, P. and Yoshimura, J., The influences of critical Moho reflections on strong ground motions recorded in San Francisco and Oakland during the 1989 Lima Prieta Earthquake. *Geophys. Res. Lett.*, 1990, **17**, 1203–1206.
22. Mori, J. and HelMBERGER, D., Large-amplitude Moho reflections (SmS) from Landers aftershocks, southern California. *Bull. Seismol. Soc. Am.*, 1996, **86**, 1845–1852.
23. Wu, F., Sheehan, A., Huang, G. C. and Monsalve, G., Source mechanisms, seismicity, and velocity structures. Indo-US Workshop on Seismicity and Geodynamics, 2003, p. 49.
24. Chander, R., Interpretation of observed ground level changes due to the Kangra earthquake, northwest Himalaya. *Tectonophysics*, 1988, **149**, 289–298.
25. Dikshit, A. M. and Koirala, A., Report on the intensity mapping of Udaypur earthquake of 20 August 1988, HMG Ministry of Industry, Nepal, Dept. of Mines and Geol., Lainchaur, Kathmandu, 1989.
26. Bihar–Nepal earthquake, 20 August 1988, GSI Special Publication, 1993, no. 31.
27. Chen, W.-P. and Kao, H., Seismotectonics of Asia: Some recent progress. In *Tectonic Evolution of Asia* (eds Yin, A. and Harrison, T. M.), Cambridge University Press, 1996, pp. 37–54.
28. Duda, S. J., Khattri, K. N., Purcaru, G. and Schick, R., Wiechert seismograms of the Goettingen Observatory – micro filming and reinterpretation. *Gerlands Beitrage zur Geophysik*, 1990, **99**, 313–336.
29. Thomas, R. H., The Magnetic Survey of India 1904–05. In Extracts from Narrative Reports of Officers of the Survey of India for the Season 1904–05, Survey of India, Government Printing Office, Calcutta, 1907.
30. Hill, D. P. *et al.*, Seismicity remotely triggered by the magnitude 7.3 Landers, California, Earthquake. *Science*, 1993, **260**, 1617–1623.
31. Bilham, R., Wallace, K., Blume, F. and Feldl, N., Flexure and fragmentation of the Indian plate: Mid-plate earthquakes, Indo-US Workshop on Seismicity and Geodynamics, National Geophysical Research Institute, Hyderabad, 2003, p. 27.

ACKNOWLEDGEMENTS. We thank an anonymous reviewer for suggestions that improved the manuscript as well as Kusala Rajendran and the staff of the NGRI for facilitating this special volume. Support for two of the authors (RB and NF) was provided by NSF EAR0003445.